HHS Public Access

Author manuscript

Circ Res. Author manuscript; available in PMC 2019 May 11.

Published in final edited form as:

Circ Res. 2018 May 11; 122(10): 1369–1384. doi:10.1161/CIRCRESAHA.117.312333.

Lysosomal Cholesterol Hydrolysis Couples Efferocytosis to Anti-Inflammatory Oxysterol Production

Manon Viaud[*], **Stoyan Ivanov**[*], **Nemanja Vujic**, **Madalina Duta-Mare**, **Lazaro-Emilio Aira**, **Thibault Barouillet**, **Elsa Garcia**, **Francois Orange**, **Isabelle Dugail**, **Isabelle Hainault**, **Christian Stehlik**, **Sandrine Marchetti**, **Laurent Boyer**, **Rodolphe Guinamard**, **Fabienne Foufelle**, **Andrea Bochem**, **Kees G. Hovingh**, **Edward B. Thorp**, **Emmanuel L. Gautier**, **Dagmar Kratky**, **Paul Dasilva-Jardine**, and **Laurent Yvan-Charvet**

Institut National de la Santé et de la Recherche Médicale (Inserm) U1065, Université Côte d'Azur, Centre Méditerranéen de Médecine Moléculaire (C3M), Atip-Avenir, Fédération Hospitalo-Universitaire (FHU) Oncoage, Nice, France (M.V., S.I., L.-E.A., E.G., S.M., L.B., R.G., L.Y.-C.); Acquire Innovation Ltd, Dublin, Ireland (T.B.); Gottfried Schatz Research Center for Cell Signaling, Metabolism and Aging, Molecular Biology and Biochemistry, Medical University of Graz, Austria (N.V., M.D.-M., D.K.); UFR Sciences, Faculté des Sciences de l'Université de Nice-Sophia Antipolis, France (F.O.); Institut National de la Santé et de la Recherche Médicale (INSERM) UMR_S 1166, Pierre & Marie Curie University, ICAN Institute of Cardiometabolism & Nutrition, Hôpital de la Pitié, Boulevard de l'Hôpital, Paris, France (I.D., E.L.G.); Institut National de la Santé et de la Recherche Médicale (Inserm) UMRS 1138, Centre de Recherche des Cordeliers, Paris, France (I.H., F.F.); Department of Pathology, Feinberg Cardiovascular Research Institute, Feinberg School of Medicine, Northwestern University, Chicago, IL (C.S., E.B.T.); Cardiology (A.B.) and Department of Vascular Medicine (K.G.H.), Academic Medical Center, Amsterdam, The Netherlands; and Staten Biotechnology, Nijmegen, The Netherlands (P.D.-J.)

Abstract

Rationale—Macrophages face a substantial amount of cholesterol after the ingestion of apoptotic cells, and the LIPA (lysosomal acid lipase) has a major role in hydrolyzing cholesteryl esters in the endocytic compartment.

Objective—Here, we directly investigated the role of LIPA-mediated clearance of apoptotic cells both in vitro and in vivo.

Methods and Results—We show that LIPA inhibition causes a defective efferocytic response because of impaired generation of 25-hydroxycholesterol and 27-hydroxycholesterol. Reduced synthesis of 25-hydroxycholesterol after LIPA inhibition contributed to defective mitochondria-associated membrane leading to mitochondrial oxidative stress–induced NLRP3 (NOD-like

Correspondence to Laurent Yvan-Charvet, PhD, Institut National de la Santé et de la Recherche Médicale (Inserm) U1065, Université Côte d'Azur, Centre Méditerranéen de Médecine Moléculaire (C3M), Atip-Avenir, Fédération Hospitalo-Universitaire (FHU) Oncoage, 06204 Nice, France. yvancharvet@unice.fr.

[*]These authors contributed equally to this article.

The online-only Data Supplement is available with this article at http://circres.ahajournals.org/lookup/suppl/doi:10.1161/CIRCRESAHA.117.312333/-/DC1.

Disclosures

None.

receptor family, pyrin domain containing) inflammasome activation and caspase-1–dependent Rac1 (Ras-related C3 botulinum toxin substrate 1) degradation. A secondary event consisting of failure to appropriately activate liver X receptor–mediated pathways led to mitigation of cholesterol efflux and apoptotic cell clearance. In mice, LIPA inhibition caused defective clearance of apoptotic lymphocytes and stressed erythrocytes by hepatic and splenic macrophages, culminating in splenomegaly and splenic iron accumulation under hypercholesterolemia.

Conclusions—Our findings position lysosomal cholesterol hydrolysis as a critical process that prevents metabolic inflammation by enabling efficient macrophage apoptotic cell clearance.

Keywords

cholesterol; inflammation; macrophage; mitochondria; oxysterols

Macrophages regulate tissue homeostasis through the uptake and catabolism of plasma lipoproteins, thus avoiding ectopic lipid deposition.[1,2] Tissue integrity also results from the efficient efferocytic capacity of macrophages to prevent the leakage of immunogenic peptides and lipid contents from dying cells.[3,4] When macrophages ingest modified lipoproteins or apoptotic cells, they increase their cellular contents and metabolic load. Excess cholesterol delivered to macrophages by these pathways must be processed within the lysosome and then re-esterified for storage leading to noncytotoxic macrophage foam cell formation.[5–7] Excess cholesterol can also be exported to extracellular acceptors via cholesterol efflux pathways to prevent the cytotoxic effects associated with elevated free cholesterol within the endoplasmic reticulum (ER) or the formation of cholesterol crystals within the lysosome.[8,9] The efflux of cholesterol is governed by liver X receptors (LXRs), which are members of the nuclear receptor superfamily that not only sense an excess of cholesterol but also regulate genes involved in anti-inflammatory responses.[7,10]

LIPA (lysosomal acid lipase) is a unique acid hydrolase enzyme that breaks down fatty material within the lysosomal compartment of cells. In humans and mice, LIPA deficiency is associated with multiple complications, including severe dyslipidemia, abnormal liver function, hepatomegaly, splenomegaly, and accelerated atherosclerosis because of the accumulation of fatty deposits and the formation of pathogenic macrophage foam cells.[11,12] Interestingly, myeloid cell–specific re-expression of LIPA in LIPA-deficient mice corrects most of their inflammatory and tissue pathogenic phenotypes.[13] This finding suggests that macrophage LIPA expression plays a nonredundant role in tissue lipid homeostasis by preventing metabolic inflammation. However, the underlying molecular mechanisms that drive this inflammation remain to be elucidated.

In macrophages, LIPA hydrolyzes not only fatty materials on CD36 scavenger receptor–mediated endocytosis to promote mitochondrial fatty acid oxidation[14] but also cholesteryl esters on the fusion of lipid droplets with lysosomes to support free cholesterol efflux, a process termed lipophagy.[15] This illustrates the pivotal role of LIPA at the interface of different catabolic pathways. Of note, the unabated uptake of modified lipoprotein-derived cholesterol and defective autophagy has been linked to sterile inflammation as a consequence of cholesterol crystal formation within macrophage lysosomes, promoting the assembly of the NLRP3 (NOD-like receptor family, pyrin domain containing)

inflammasome and activation of caspase-1.[16,17] Although a protective role of LIPA in macrophages during acute parasitic infection has recently emerged,[14] the contribution of LIPA-dependent processing of cholesteryl esters in sterile inflammation remains elusive.

To test the causal relationship between lysosomal cholesterol processing and macrophage function, we explored the role of LIPA after engulfment of apoptotic cells. We report here that LIPA is critical for efficient efferocytosis. These effects were mediated not by defective LC3-associated phagocytosis-engaged phagosome (LAPosome) formation or lysosomal dysfunction. We rather report that LIPA controls the generation of 25- and 27-hydroxycholesterol (OHC). Reduced 25-OHC after LIPA inhibition contributed to defective mitochondria-associated membrane (MAM)–dependent mitochondrial metabolic repurposing leading to the activation of the NLRP3 inflammasome after efferocytosis. Activation of the inflammasome subsequently promoted defects in Rac1 (Ras-related C3 botulinum toxin substrate 1)-dependent phagocytic cup formation. Reduced 25- and 27-OHC also contributed to dampen LXR activation causing mitigation of cholesterol efflux and apoptotic cell clearance. In vivo experiments confirmed that LIPA inhibition led to defective clearance of apoptotic cells and stressed erythrocytes by splenic and hepatic macrophages. This process culminated in splenomegaly and splenic iron accumulation under hypercholesterolemic conditions. Our data highlight that LIPA is integral to macrophage efferocytic response, and they provide a framework for understanding the contribution of LIPA to chronic inflammation.

Methods

All data and methods used in the analysis and materials used to conduct the research will be made available to any researcher for the purpose of reproducing the results or replicating the procedures.

All data, methods, and materials are available on personal request at the University Côte d’Azur, Center Méditerranéen de Médecine Moléculaire (L.Y.-C).

An expanded Methods section is available in the Online Data Supplement.

Animals and Treatments

Wild-type and Ldlr$^{-/-}$ mice in a C57BL6/J background were obtained from the Janvier Laboratory (Saint Berthevin, France) and fed a normal chow diet. Hyperlipidemia was induced by feeding the mice with a Western diet (TD88137, Ssniff) for 12 weeks. Two weeks before the end of the study, mice were challenged with subcutaneous injections every 2 days of 20 mg/kg lalistat (Enamine) solubilized in 0,5% methylcellulose 0,1% Tween 20 or with control solution. Mice were euthanized 1 day after the last injection. All animals procedures were approved by the Institutional Animal Care and Use Committee of the French Ministry of Higher Education and Research and the Mediterranean Center of Molecular Medicine (Inserm U1065) and were undertaken in accordance with the European Guidelines for Care and Use of Experimental Animals. Animals had free access to food and water and were housed in a controlled environment with a 12-hour light–dark cycle and constant temperature (22°C).

Results

Optimal Clearance of Apoptotic Cells Depends on LIPA

We first made the observation that opposing regulation of LIPA activity occurred between classical (lipopolysaccharide) and alternative (IL [interleukin]-4) macrophage activation, and this correlated with the efferocytic capacity of these cells (Figure 1A). Thus, we examined whether LIPA could impact efferocytosis in human THP-1 macrophages. Efferocytosis was analyzed 30 minutes after exposure to apoptotic Jurkat cells in LIPA-deficient cells (LIPA knockdown using siRNA or lentiviral ShRNA particles; Online Figure IA) or LIPA-overexpressing cells (Ovex, using stable transfection; Online Figure IB). Remarkably, LIPA expression modulated optimal engulfment of apoptotic cells as shown after knockdown or overexpression (Figure 1B). These efferocytic responses paralleled BODIPY (bore-dipyrromethene)-neutral lipid stainings in both LIPA-deficient and LIPA-overexpressing THP-1 macrophages 30 minutes after ingestion of apoptotic cells (Figure 1C). LIPA inhibition was next achieved with lalistat. A time-course experiment showed that the efferocytic index was unaffected by lalistat 3 and 6 hours post-efferocytosis in THP-1 macrophages but was significantly reduced by 46% 24 hours after efferocytosis (Figure 1D and 1E). Consistently, reduced phagocytic capacity was also observed in LIPA-deficient murine bone marrow–derived macrophages, and lalistat treatment did not show any additive effects in these cells (Online Figure IC). These results reveal that LIPA inhibition initiates a sequential cascade of events that leads to impaired efferocytic response. Importantly, quantification of BODIPY staining in a time-course experiment revealed that neutral lipid accumulation preceded defects observed on efferocytosis after LIPA inhibition both in THP-1 macrophages (Figure 1F) and murine primary macrophages (Online Figure ID). Thus, LIPA-dependent clearance of apoptotic cells is most likely the consequence on how efferocytes initially handle cholesterol, the main neutral lipid in macrophages.

LIPA Controls Lysosomal Cholesterol Trafficking During Efferocytosis

To better comprehend the mechanism by which LIPA modulates the efferocytic response, we performed an assay to follow the diffusion of cholesterol within intracellular compartments. Human THP-1 macrophages that had been cultured for 1 hour after the ingestion of [^{3}H]-cholesterol–prelabeled apoptotic Jurkat cells were fractionated by sucrose step gradient, and cellular fractions were assayed for [^{3}H]-cholesterol levels. The accumulation of cholesterol was observed 1 hour after efferocytosis in the high-density membrane fraction (enriched in endosomes and lysosomes) and in the plasma membrane fraction of lalistat-treated efferocytes (Figure 1G). In contrast, reduced cholesterol content in high-density membrane fraction was observed 1 hour after the ingestion of [^{3}H]-cholesterol–prelabeled apoptotic Jurkat cells in LIPA-overexpressing cells (Online Figure IE). As expected, cholesteryl esters accumulated in the high-density membrane fraction after LIPA inhibition and to some extent in the plasma membrane fraction (Online Figure IF). At this time point, there was no significant difference in the amount of cholesterol diffusing in the Golgi but less diffusion of free cholesterol occurred in the ER fraction in lalistat-treated THP-1 macrophages compared with control cells (Figure 1G; Online Figure IF). Consistent with the accumulation of cholesteryl esters rather than free cholesterol after LIPA inhibition, transmission electron microscopy revealed only sparse cholesterol crystal formation in lalistat-treated THP-1

macrophages (1 identified among >400 visualized lysosomes with similar structures; Online Figure IG). However, we observed almost complete absence of whorl-shaped lysosomes in these cells compared with control cells (Online Figure IG, right), providing ultrastructural evidence of altered lysosomal lipid composition. To strengthen these observations, human THP-1 macrophages were cocultured in vitro with BODIPY-prelabeled apoptotic Jurkat cells in the presence or absence of lalistat and confocal microscopy was performed to visualize the diffusion of cholesterol within intracellular compartments. LysoTracker staining (red) revealed that a considerable amount of BODIPY (green) was localized in the phagolysosomal membrane surrounding the apoptotic cells (yellow staining: overlap between green apoptotic cells and red LysoTracker staining) in lalistat-treated efferocytes (Online Figure IH). In contrast, BODIPY (green) diffused within intracellular compartments in control and LIPA-overexpressing THP-1 efferocytes (Online Figure IH). Performing 3-dimensional reconstruction from confocal Z-stack images more clearly revealed the BODIPY lining surrounding apoptotic cells in lalistat-treated THP-1 efferocytes (Figure 1H). Thus, LIPA is a key lysosomal enzyme that processes cholesteryl esters ingested from apoptotic cells during efferocytosis.

Defective Lysosomal Cholesterol Hydrolysis Does Not Initiate LAP or Lysosomal Dysfunction After Efferocytosis

During phagocytosis, LAP (microtubule-associated protein 1A/1B-light chain 3 (LC3)-associated phagocytosis) is a process by which LC3-II conjugation to phagosomes enables phagosome–lysosome fusion, stabilization of the NOX2 (NADPH oxidase 2) complex and apoptotic cell corpse clearance,[18] and we previously reported that NOX2 translocates to phagolysosomes in a cholesterol-dependent fashion.[19] Western blot analysis of LC3-II/LC3-I ratio showed that inhibition of LIPA in THP-1 macrophages did not alter LAP-engaged phagosome between 0 and 6 hours after efferocytosis (Figure 2A and 2B). Although both LC3-I and LC3-II forms were reduced in LIPA-overexpressing THP-1 macrophages, the LC3-II/LC3-I ratio was also not significantly modified between 0 and 6 hours after efferocytosis (Online Figure IIA). We also investigated active NOX complex formation by immunostaining for p47^{phox} clustering, one of the active components of the NOX2 complex. As expected, a considerable amount of p47^{phox} staining (red) was localized to phagolysosomal membranes surrounding the apoptotic cells 1 hour post-efferocytosis; however, quantification of the phagolysosomal p47^{phox} staining did not reveal any difference between the control and lalistat-treated macrophages (Online Figure IIB). Consistent with the role of the NOX complex in controlling phagolysosomal pH,[18] similar lysosomal acidification was observed between control and lalistat-treated efferocytes as measured by confocal microscopy 1 hour after the ingestion of apoptotic cells (Online Figure IIC) or by flow cytometry using a LysoSensor probe (Online Figure IID). LIPA-overexpressing THP-1 macrophages also exhibited similar lysosomal acidification response (Online Figure IID). Altogether, our data indicate that defective lysosomal cholesterol hydrolysis does not initiate phagolysosome dysfunction after efferocytosis.

Defective autophagy or lysosomal biogenesis promotes macrophage apoptosis,[16,20,21] and we previously reported that defective efferocytosis could be the consequence of an excess cholesterol accumulation that induces apoptosis.[19] Western blot analysis revealed an

increase in LC3II/LC3-I ratio 24 hours post-efferocytosis in lalistat-treated THP-1 macrophages, indicative of an enhanced autophagic response (Figure 2A and 2B). We also observed an increased number of lysosomes in lalistat-treated THP-1 macrophages 24 hours post-efferocytosis using the LysoTracker probe and flow cytometry (Online Figure IIE). The dephosphorylated form of TFEB (transcription factor E-box) is essential for optimal TFEB activation through translocation into the nucleus and subsequent activation of a gene network regulating lysosomal biogenesis and autophagy.[22] Inhibition of LIPA in macrophages led to an increase in the dephosphorylated form of TFEB 24 hours after ingestion of apoptotic cells (Figure 2A and 2B), evoking an adaptive rather than a defective lysosomal biogenesis or autophagic response. Consistently, apoptosis was unaffected in LIPA-deficient THP-1 efferocytes (LIPA knockdown using siRNA or lentiviral ShRNA particles) or lalistat-treated THP-1 efferocytes (Online Figure IIF). In contrast, LIPA-overexpressing efferocytes exhibited lower autophagic and lysosomal biogenesis responses as shown by reduced expression of the dephosphorylated form of TFEB and both forms of LC3-I and LC3-II (Online Figure IIA) and reduced LysoTracker staining (Online Figure IIE). However, apoptosis was also unaffected in these cells (Online Figure IF). Thus, lysosomal cholesterol hydrolysis capacity dictates TFEB-dependent lysosomal biogenesis, and this adaptive compensatory response is unlikely the cause of defective efferocytosis but rather prevents macrophage from apoptosis.

Activation of the NLRP3 Inflammasome Causes Defective Efferocytosis After LIPA Inhibition

To evaluate whether LIPA-dependent lysosomal cholesterol storage ties lysosomal inflammation,[23] to defective efferocytosis, we next assessed the secretion of lysosomal inflammatory markers cathepsin B, K, and IL-1β after ingestion of apoptotic cells. Consistent with the absence of lysosomal damage after LIPA inhibition, similar secretion of cathepsin B and K was observed between control and lalistat-treated THP-1 efferocytes (Figure 2C; Online Figure IIA). However, higher IL-1β and IL-18 secretion was observed 3 hours after LIPA inhibition in THP-1 efferocytes (Figure 2D). Similar findings were observed after LIPA inhibition in murine thioglycollate-elicited peritoneal efferocytes (Online Figure IIIB). The NLRP3 inflammasome, which is a well-known sensor of danger signals, is involved in caspase-1–dependent maturation and secretion of IL-1β and IL-18.[24] Consistently, an inhibitor of NLRP3 (CP-456773) prevented the enhanced IL-1β and IL-18 secretion in lalistat-treated THP-1 efferocytes (Figure 2D). Reduced IL-1β secretion, but not cathepsin B, was also observed in LIPA-overexpressing THP-1 efferocytes (Figure 2C; Online Figure IIIC). A time-course experiment confirmed an 100% increase in caspase-1 cleavage in THP-1 efferocytes as early as 3 hours after lalistat treatment, and this was sustained up to 24 hours after the ingestion of apoptotic Jurkat cells in lalistat-treated efferocytes (Figure 2E). This result was associated with an increase in FAM (carboxyfluorescein)-Flica caspase-1 activity that could be prevented by the NLRP3 inhibitor (Online Figure IIID). Using immortalized murine NLRP3-deficient macrophages, we confirmed the dependence of the NLRP3 inflammasome on IL-1β secretion (Online Figure IIIE) and caspase-1 activation (Online Figure IIIF) after LIPA inhibition. Inhibition of the NLRP3 inflammasome partially restored the efferocytic index of lalistat-treated THP-1 efferocytes (Figure 2F). CP-456773 treatment and caspase-1 deficiency also

prevented the efferocytosis defect induced by LIPA inhibition in murine thioglycollate-elicited peritoneal efferocytes (Online Figure IIIG). Thus, lysosomal cholesterol hydrolysis prevents the NLRP3 inflammasome–activating danger signal during efferocytosis to allow efficient clearance of apoptotic cells.

Caspase-1 activation has been previously proposed to cleave Rac1,[25] which is a canonical Rho guanosine triphosphate (GTPase) involved in cytoskeletal reorganization and efferocytosis.[26] Transmission electron microscopy showed that the morphology of lalistat-treated THP-1 efferocytes differed from control cells after 24 hours of culture with a less identifiable phagocytic cup that transform from filopodia and underlying lamellipodia (Online Figure IIIH). Immunostaining for Rac1 (green) and F-actin (red) 6 hours after efferocytosis revealed a considerable amount of costaining at the leading edge of membrane ruffle formation surrounding the apoptotic cells in control macrophages (overlapping yellow staining; Online Figure IIII, upper). In contrast, a general decrease in phagolysosome Rac1 was observed after LIPA inhibition (Online Figure IIII, lower). This was more clearly visible after we performed 3-dimensional reconstruction from confocal Z-stack images (Figure 2G). Reduced Rac1 protein expression was confirmed in THP-1 efferocytes after LIPA inhibition by Western blot (Figure 2H). Pull-down activation assay confirmed reduced Rac1 activity after LIPA inhibition (Figure 2H). To determine when after LIPA inhibition this decline in cell ruffling occurs, we used impedance to perform real-time monitoring of cell protrusion dynamics.[27] These analyses revealed increased resistance in lalistat-treated THP-1 macrophages beginning 6 hours post-efferocytosis (Figure 2I), a signature that followed the inflammasome activation. We confirmed that the Rac1 inhibitor NSC23766, known to selectively lower active Rac1-GTP levels, also increased resistance in control cells to the level of lalistat-treated efferocytes (Figure 2I). Inhibition of the NLRP3 inflammasome (CP-456773 treatment) rescued Rac1 protein expression (Figure 2H). These findings provide a mechanism by which inflammasome-activating danger signal contributes to the defective efferocytic response after LIPA inhibition.

Defective Lysosomal Cholesterol Hydrolysis Repurposes MAM-Dependent Mitochondrial Metabolism to Activate the NLRP3 Inflammasome and Dampen Efferocytosis

Recent evidence suggests that LIPA is important for mitochondrial oxidative phosphorylation,[15] and elevated mitochondrial reactive oxygen species (ROS) production has been proposed to activate the NLRP3 inflammasome.[28] Reduced metabolic flux in the mitochondria of lalistat-treated THP-1 efferocytes was reflected by a decrease in the oxygen consumption rate at baseline or after the inhibition of oxidative phosphorylation by oligomycin treatment (Figure 3A; Online Figure IVA). The enhanced oxygen consumption rate response was also prevented in thioglycollate-elicited peritoneal efferocytes after LIPA inhibition or in LIPA-deficient efferocytes (Online Figure IVB). The increased capacity of LIPA-overexpressing THP-1 cells to capture and take up apoptotic Jurkat cells was also associated with increased oxygen consumption rate and maximal respiration response after FCCP (carbonyl cyanide 4-[trifluoromethoxy] phenylhydrazone) treatment (Figure 3A). These observations were further supported by reduced mitochondrial uncoupling protein 2 (*ucp2*) mRNA expression in lalistat-treated THP-1 efferocytes (Online Figure IVC) and enhanced mRNA levels of heme oxygenase-1 (*Hmox1*; Online Figure IVD) starting 1 hour

after efferocytosis. Reduced mitochondrial flux and uncoupling of lalistat-treated THP-1 efferocytes paralleled an increase in mitochondrial ROS generation (Figure 3B and 3C). This effect was most likely because of a raise in mitochondrial potential ($\Delta\Psi_m$) because the addition of the complex I inhibitor (rotenone), the complex II inhibitor (3-nitropropionic acid), or the succinate oxidation inhibitor (dimethyl malonate) promoted mitochondrial ROS production in control cells but not in lalistat-treated THP-1 efferocytes (Figure 3C). These inhibitors also resulted in an increase in IL-1β secretion in control but not in lalistat-treated efferocytes (Figure 3D).

Calcium is a central player in mitochondria metabolic repurposing and inflammasome activation,[29,30] and different lysosomal storage diseases have been associated with calcium flux modulation.[31–33]

We first activated the 2 main lysosomal calcium pathways, the nicotinic acid adenine dinucleotide phosphate receptor with the membrane-permeant NAADP (nicotinic acid adenine dinucleotide phosphate) analog (NAADP-AM [acetoxymethyl]) and the mucolipin TRPML1 (transient receptor potential channel 1) with the mucolipin synthetic agonist. However, these treatments did not modify FAM-Flica caspase-1 activity or IL-1β secretion (Online Figure IVE and IVF). In contrast, activation of the mitochondrial IP3R (inositol trisphosphate receptor) with low-dose 2-aminoethyl diphenylborinate completely prevented the inflammasome activation and IL-1β secretion in lalistat-treated efferocytes (Online Figure IVE and IVF). These findings suggest that inhibition of LIPA promotes mitochondrial metabolic repurposing-dependent inflammasome activation by limiting mitochondrial calcium flux. To directly test this hypothesis, efferocytes were loaded with the calcium probe Fluo4-AM and calcium release from the mitochondria, a surrogate of mitochondrial calcium content, was assessed after treatment of cells with the mitochondrial uncoupler, carbonyl cyanide 3-chlorophenylhydrazone. We observed a striking decrease in mitochondrial calcium release in lalistat-treated THP-1 efferocytes compared with control cells (Figure 3E). Calcium-dependent activation of the inflammasome relies on MAMs that comprise IP3R and chaperone proteins.[30] Transmission electron microscopy highlighted ER–mitochondria contacts in control THP-1 efferocytes, an effect that was less visible in lalistat-treated cells (Figure 3F). The ER-localized chaperone GRP78 (78 kDa glucose-regulated protein; BiP [binding immunoglobulin protein]) is part of the MAM macromolecular complex and interacts with ER lipid transporters.[34] Overexpression of GRP78 normalized the mitochondrial calcium response of lalistat-treated THP-1 efferocytes (Figure 3E) and prevented the exacerbated IL-1β secretion (Figure 3G). Consistently, GRP78 overexpression also restored efficient efferocytosis in lalistat-treated efferocytes (Figure 3H). Thus, we propose that LIPA is required for MAM-dependent calcium flux after efferocytosis. This flux will repurpose the mitochondria to limit the inflammasome-activating danger signal and allow efficient efferocytosis.

LIPA Primes the Sterol-Dependent Metabolic Reprogramming of Efferocytes

The group of Cyster recently reported that defective 25-OHC generation in the ER promotes inflammasome activation in macrophages.[35,36] Thus, we next quantified sterol metabolites using liquid chromatography-mass spectrometry in control and lalistat-treated THP-1

macrophages 3 hours post-efferocytosis. Precursors of cholesterol synthesis such as lanosterol, 24-DH (dehydro)-lanosterol, 7-DH cholesterol, and desmosterol and toxic sterols such as α-triols (cholesterol-3β,5α,6β-triol), α-Epox (cholesterol-5α,6α-epoxide), 7α-OHC, and 7-ketocholesterol were not altered at this time point in lalistat-treated efferocytes (Online Figure VA and VB). The brain-specific 24S-OHC was near the detection limit and was unaltered in lalistat-treated efferocytes (Figure 4A). In contrast, a striking 50% to 70% decrease in oxysterols made from free cholesterol in the ER, such as 4β-OHC and 25-OHC, or in the mitochondria, such as 27-OHC, was observed in lalistat-treated efferocytes (Figure 4A). These decreases were not associated with significant changes in the mRNA expression of the related oxysterol biosynthetic enzymes in lalistat-treated efferocytes (Online Figure VC), suggesting that LIPA inhibition impacts the production of oxysterols by limiting substrate availability.

Part of the mechanism by which defective 25-OHC generation activates the inflammasome relies on modulation of cholesterol biosynthetic genes.[35,36] The ingestion of apoptotic cells led to a decrease in the mRNA expression of the biosynthetic genes *Srebf2* and *Hmgcr* in control macrophages starting 3 hours after efferocytosis, an effect that was virtually absent in lalistat-treated THP-1 macrophages (Figure 4B; Online Figure VD and VE). In contrast, *Srebf2* and *Hmgcr* mRNA expression were further intensified in LIPA-overexpressing THP-1 macrophages 3 hours after efferocytosis (Figure 4B). Treatment of the cells with 25-OHC restored the downregulation of *Srebf2* and *Hmgcr* mRNA expression in lalistat-treated efferocytes (Figure 4B). These findings suggest that cholesteryl ester hydrolysis of engulfed apoptotic cells favors the flux of free cholesterol toward the ER (Online Figure IE) to generate 25-OHC and dampen cholesterol biosynthetic pathway after efferocytosis. Treatment with 25-OHC partially restored the decrease in oxygen consumption rate observed in lalistat-treated THP-1 efferocytes (Figure 4C) and rescued their mitochondrial calcium defect (Figure 4D), offering a potential mechanism by which 25-OHC could control ER-dependent mitochondrial proticity after efferocytosis. Consistently, treatment with 25-OHC reduced inflammasome activation after efferocytosis in lalistat-treated THP-1 macrophages, as reflected by reduced IL-1β secretion (Figure 4E) and restored an efficient efferocytic response (Figure 4F). Treatment of LIPA-deficient murine macrophages with 25-OHC also rescued the defective efferocytosis of these cells (Online Figure VF). The reduced IL-1β secretion in LIPA-overexpressing efferocytes was also abolished after knockdown of Ch25h by siRNA (Online Figure VG). Thus, we propose that impaired 25-OHC generation after LIPA inhibition controls mitochondrial metabolic repurposing to activate the inflammasome and limit subsequent clearance of apoptotic cells.

25-OHC and 27-OHC are potent endogenous LXR agonists, and LXR activation occurs after efferocytosis to support efficient efferocytosis through upregulation of cholesterol efflux transporters or the efferocytic receptor *MertK*.[19,37] Thus, we next examined the expression of LXR target genes during the course of efferocytosis and observed that the mRNA expression of the cholesterol efflux transporters *Abca1* (ATP-binding cassette A1) and *Abcg1* (ATP-binding cassette G1) was not altered in the early phase of efferocytosis in lalistat-treated THP-1 macrophages (up to 6 hours) but was significantly decreased in the late resolution phase (Online Figure VIA and VIB). Cholesterol efflux studies have confirmed a decrease in cholesterol efflux to lipid-poor apoA-1 (apolipoprotein A1), the

major apolipo-protein of HDL (high-density lipoprotein; Online Figure VIC) and to PEG (polyethylene glycol)-HDL (Online Figure VID) 24 hours after the ingestion of apoptotic cells in lalistat-treated THP-1 macrophages. In contrast, LIPA-overexpressing THP-1 efferocytes exhibited higher mRNA expression of LXR target genes (Online Figure VIE) and more cholesterol efflux to PEG-HDL (Online Figure VIF). We confirmed the LXR dependency of these effects, as treatment with the synthetic LXR agonist TO901317 enhanced not only the expression of *Abca1* and *Abcg1* (Online Figure VIG) but also cholesterol efflux to HDL in lalistat-treated THP-1 macrophages (Online Figure VIH). Consistently, we observed reduced mRNA expression of the efferocytic receptor *MertK* in lalistat-treated THP-1 macrophages 24 hours after efferocytosis (Figure 4G). In contrast, *MertK* was upregulated in LIPA-overexpressing THP-1 efferocytes (Online Figure VIE). To delineate whether LXR activation could rescue the adverse effects of LIPA inhibition on efferocytes, stimulation of LXR activity was achieved with 25-OHC, 27-OHC, or the synthetic LXR agonist TO901317 for 24 hours. In contrast to 25-OHC treatment, 27-OHC or TO901317 did not prevent the inflammasome activation (Figure 4E). However, all treatments enhanced *MertK* mRNA expression in control and lalistat-treated THP-1 efferocytes (Figure 4G). This could explain how 27-OHC and TO901317 partially restored the efferocytic capacity of lalistat-treated efferocytes (Figure 4F). The relevance of this pathway was further illustrated through the effect of the LXR agonist in synergizing with the NLRP3 inhibitor (CP-456773) to fully restore efficient efferocytosis (Figure 4H). These results indicate that LXR activation is a critical checkpoint by which LIPA controls the efferocytic response.

Altogether, these findings reveal that LIPA favors efficient efferocytosis through sterol-dependent metabolic reprogramming: (1) the ER-dependent 25-OHC generation after lysosomal cholesterol hydrolysis will limit inflammasome-activating danger signal and prevent Rac1-dependent phagocytic cup disassembly and (2) 25- and 27-OHC generation after lysosomal cholesterol hydrolysis will activate an LXR-dependent transcriptional program that favors ABCA1- and ABCG1-dependent efflux of cholesterol ingested from apoptotic cells and primes efferocytes for multiple MertK-dependent clearance of apoptotic cells.

LIPA Orchestrates Disposal of Stressed Erythrocytes and Apoptotic Cells In Vivo

Taking advantage of a publicly available gene expression data set from Immgen (http://immgen.org), we observed that efferocytosis markers, LXR target genes, and heme and iron homeostasis markers were predominantly expressed not only in peritoneal macrophages but also in specialized tissue-resident macrophages, paralleling LIPA expression and lysosome markers (Online Figure VIIA). This finding suggested an important interplay between LIPA, cholesterol homeostasis, and tissue-resident macrophage lysosomal and erythrophagocytic functions. The in vivo contribution of LIPA to efferocytosis was next studied using 2 different models. The use of lalistat treatment over LIPA-deficient mice was chosen to avoid an inflammatory phenotype that could origin from embryogenesis.[12] We intravenously injected either fluorescently labeled stressed erythrocytes (stressed red blood cells [sRBCs]) or apoptotic lymphocytes (ALs) into mice treated with lalistat or vehicle for 2 weeks and examined their macrophage efferocytic capacity in spleen and liver 16 hours later. sRBCs

and ALs were retrieved in the liver and spleen (Online Figure VIIB) and accumulated within different leukocyte populations gated by flow cytometry as $CD11b^{lo}F4/80^{int}$ myeloid cells, $CD11b^{lo}F4/80^{high}$ Kupffer cells (KCs) or red pulp macrophages (RPMs), and $CD11b^{high}F4/80^{high}$ whether these cells are the newly identified transient macrophage population (T-macs) or a subpopulation of myeloid cells (Figure 5A).[38] In the liver, sRBCs and to a lesser extent ALs promoted the appearance of T-macs or a subpopulation of myeloid cells (Figure 5A). Both T-macs and KCs ingested labeled sRBCs or ALs (Figure 5B; Online Figure VIIC). A small fraction of myeloid cells also ingested fluorescent sRBCs or ALs (Figure 5B; Online Figure VIIC). Lalistat treatment reduced the ability of KCs and T-macs to phagocytose labeled sRBCs and ALs (Figure 5B; Online Figure VIIC). However, lalistat also induced a compensatory increase in the number of myeloid cells that had phagocytosed labeled ALs (Online Figure VIIC). In the spleen, RPMs were the most abundant cell population that efficiently cleared labeled sRBCs and ALs (Figure 5C; Online Figure VIID). Lalistat treatment reduced the efferocytic capacity of RPMs (Figure 5C; Online Figure VIID), and there was a specific compensatory upregulation of the number of myeloid cells that had ingested ALs (Online Figure VIID). The enhanced number of immature myeloid cell with efferocytic capacity after lalistat treatment was a specific response to the injection of ALs, most likely reflecting the initiation of an inflammatory response secondary to release of find-me or danger signals in this context.[27] We thus conclude that LIPA promotes the disposal of stressed RBCs and apoptotic cells in hepatic and splenic macrophage populations.

LIPA Inhibition Precipitates Hypercholesterolemia-Associated Efferocytosis Defects

Previous studies have documented defective efferocytosis and splenomegaly under hypercholesterolemic conditions.[2] Thus, high-fat diet-fed hypercholesterolemic *Ldlr*$^{-/-}$ mice were next treated with lalistat for 2 weeks. An analysis of macrophage numbers in the spleen (RPMs), liver (KCs), adipose tissue macrophages, and peritoneal macrophages (Online Figure VIIIA) revealed a specific increase in RPMs and KCs, probably to compensate for efferocytosis defects, but not in adipose tissue macrophages or peritoneal macrophages (Online Figure VIIIB). Consistent with this observation, reduced mRNA expression of efferocytic markers (ie, MertK, Axl, and Gas6) was downregulated by lalistat treatment along with enhanced inflammatory markers including Il1β (Figure 5D). RPMs from lalistat-treated animals also exhibited reduced cell surface expression of CD206 (the mannose receptor C-1 [MRC1]; Online Figure VIIIC). Mechanistically and in line with our in vitro studies, LIPA inhibition led to a compensatory increase in lysosomal biogenesis in RPMs and KCs with no changes in lysosomal acidification as quantified by flow cytometry (Online Figure VIIID). This result correlated with enlarged spleen and higher splenic IL-1β levels in lalistat-treated animals, whereas other inflammatory parameters were unaffected (Table). Senescent RBCs are normally phagocytosed by macrophages in the spleen and liver, and defective erythrophagocytosis leads to splenic iron deposition.[39,40] Thus, we assessed iron stores in lalistat-treated animals. Splenic iron accumulation was histologically evident and was largely confined to the red pulp in lalistat-treated animals (Figure 5E). Plasma, liver, and adipose tissue iron and ferritin concentrations were normal in lalistat-treated animals (Figure 5F and 5G; Table), but an increased iron concentration was confirmed in the spleen (Figure 5F). Ferritin concentrations were also increased by >200% in the spleens of lalistat-treated

animals but did not reach statistical significance (P=0.07; Figure 5G). Thus, our data support a critical in vivo role of LIPA in the efferocytic capacity of tissue-resident macrophages under hypercholesterolemic conditions, which is required for tissue integrity by maintaining immune and tissue lipid homeostasis.

Discussion

Macrophage lipid accumulation and defective clearance of apoptotic cells are central events in many metabolic disorders. However, the specific molecular mechanisms linking lipid accumulation to inflammation in macrophages are still not completely understood. We have now uncovered a novel mechanism by which LIPA controls macrophage inflammatory response by limiting continued clearance of apoptotic cells. Notably, our mechanistic studies demonstrated that lysosomal cholesterol hydrolysis mediated by LIPA orchestrated the timely production of 25-OHC and 27-OHC during efferocytosis, which modulated inflammasome activation and the generation of endogenous LXR ligands. Although activation of the inflammasome after LIPA inhibition led to defects in Rac1-dependent phagocytic cup formation, decreased production of LXR ligands resulted in reduced cholesterol efflux and *MertK* expression impeding subsequent apoptotic cell clearance (Figure 6). Importantly, our findings indicate that in vivo inhibition of this pathway reduced the clearance of ALs and stressed erythrocytes by splenic- and hepatic-resident macrophages leading to splenomegaly and splenic iron accumulation on hypercholesterolemic challenge. Collectively, these findings demonstrate the importance of macrophage lysosomal cholesterol hydrolysis linking metabolism and inflammation under homeostatic and disease conditions.

It has been shown that LIPA is essential for breaking down fatty material within the lysosomal compartment of macrophages on receptor-mediated endocytosis of lipoprotein, lysosome biogenesis, or lipophagy,[14,15,20] but the relevance to efferocytosis has not yet been addressed. Our findings reveal that LIPA activity follows the efferocytic capacity of polarized macrophages and controls the lysosomal degradative capacity under nonpolarizing culture conditions raising several interesting questions for future study. First, the dual role of LIPA for optimal alternative macrophage activation,[14] and efferocytosis, as detailed in the present study, might be interconnected in vivo to promote tissue repair and metabolic homeostasis.[1] The findings of reduced LIPA activity in classically activated macrophages and enhanced inflammasome activation after LIPA inhibition also indicate that LIPA might be more susceptible to exogenous inflammatory stimuli. Thus, it will be of interest to determine whether LIPA may prime macrophages prior activation. Indeed, a switch between classically and alternatively activated macrophages was previously associated to different oxidative stress responses that prime macrophage prior activation.[41,42]

Second, why enhanced oxidative stress does not initiate apoptosis after LIPA inhibition needs to be defined. Although our data exclude a role of NOX in promoting cholesterol-dependent apoptosis susceptibility,[19] they do not rule out why mitochondrial oxidative stress and associated inflammasome activation are not linked to pyroptosis or other forms of apoptosis. One explanation could be the absence of second signals that triggers apoptosis (2-hit models)[8] or the level of aggressiveness of the first signal. For instance, we found

occasional cholesterol crystals in macrophages after LIPA inhibition and no sign of lysosomal damage after apoptotic cell clearance despite higher NLRP3 inflammasome activation. These findings contrast with the activation of the NLRP3 inflammasome by cholesterol crystals relying on lysosomal damage and the subsequent proteolytic activation of cathepsins.[9,17] This could be the consequence of an accumulation of cholesteryl ester after LIPA inhibition rather than free cholesterol, which is the source of cholesterol crystal formation in lysosomes.[43] Another possibility for the lack of apoptosis induction after LIPA inhibition could involve formation of new lysosomes to face cholesterol accumulation that has been previously shown to prevent cell death.[21] It also remains an open question as to how exactly the origin and level of mitochondrial ROS, which depends on the balance between the reverse electron transport of the electron transport chain and the mitochondrial potential ($\Delta\psi_m$),[44] leads to oxidative damage to DNA, proteins, and lipids and subsequent apoptosis. It would be of interest to determine whether absence of ROS-mediated mtDNA release after LIPA inhibition may have limited activation of the AIM2 (absent in melanoma 2) inflammasome under efferocytic condition because AIM2 has redundant function with the NLRP3 inflammasome,[36] and activates apoptosis.

How does LIPA control optimal clearance of apoptotic cells? Our findings suggest that inhibition of lysosomal cholesteryl ester hydrolysis limited the generation of free cholesterol that could reach sites of oxysterol generation after the digestion of apoptotic cells. These oxysterols include 25-OHC and 27-OHC that could prime efferocytes for subsequent apoptotic cell clearance by at least 2 independent mechanisms. We first observed an unexpected mechanism that involves defective production of 25-OHC in the ER, which impaired the repression of cholesterol biosynthetic genes post-efferocytosis but also prevented MAM-dependent mitochondrial metabolic repurposing and subsequent activation of the inflammasome. This activation reduced Rac1 activity and subsequently disorganized phagocytic cups. Although it was recently shown that defective 25-OHC generation in macrophages promotes inflammasome activation,[35,36] the present study positions this observation in the context of efferocytosis and provides new insights into the underlying mechanisms. Indeed, we found that (1) LIPA controls the generation of 25-OHC after efferocytosis and (2) 25-OHC controls the MAM-dependent calcium flux to repurpose mitochondrial metabolism. Under normal physiological conditions, calcium primarily promotes ATP synthesis by stimulating enzymes of the Krebs cycle and oxidative phosphorylation in the mitochondria. This increased metabolic rate would consume more oxygen resulting in increased respiratory chain electron leakage and mitochondrial ROS levels as it is observed in control efferocytes. After LIPA inhibition, reduced mitochondrial calcium influx may have dampened oxidative phosphorylation and UCP (uncoupling protein)-2–dependent proton leaks across the inner mitochondrial membrane but at the same time reduced $\Delta\Psi_m$ consumption exacerbating mitochondrial ROS generation.[28,29] Restoring MAM-dependent calcium flux through GPR78 overexpression was sufficient to prevent the inflammasome activation after LIPA inhibition mimicking the effect of 25-OHC. Future studies will be required to understand whether MAM formation during efferocytosis is also linked to mitochondrial fission.[45] Nevertheless, this mitochondrial checkpoint is crucial for the efferocytic response of macrophages as the inflammasome activation after LIPA inhibition reduced Rac1 expression and activity. Decreased levels of Rac1 and F-actin

polymerization in membrane ruffles after the ingestion of apoptotic cells caused cytoskeletal changes and impaired pseudopod formation. Similar modulation of focal adhesion dynamics was previously observed under cholesterol-loading conditions in LIPA-deficient cells.[46] In our setting, this modulation contributed to reduce efferocytic capacity after LIPA inhibition.

Consistent with 25-OHC and 27-OHC being potent LXR agonists in macrophages,[7,10] we next observed a delayed response in LXR target gene activation after LIPA inhibition in efferocytes leading to impaired cholesterol efflux and reduced efferocytic capacity.[19,37] We confirmed that reduced LXR activation was independent of, and synergized with, the modulation of Rac1 signaling pathway to impede efficient apoptotic cell clearance.[47] Interestingly, in other lysosomal storage diseases such as Niemann-Pick type C disease, in which cholesterol accumulates within late endosomes, it has been reported that Niemann-Pick type C cells exhibit a defect in 25-OHC and 27-OHC in response to LDL (low-density lipoprotein) and fail to repress SREBPs (sterol regulatory element-binding proteins) and LXRs.[48,49] Our findings extend these observations, and we propose that LIPA-dependent cholesteryl ester hydrolysis, which is upstream of endosomal Niemann-Pick type C–dependent cholesterol trafficking, might be an earlier enzymatic step that governs oxysterol generation and LXR activation during efferocytosis. Thus, LIPA-dependent lysosomal cholesterol hydrolysis orchestrates the timely cholesterol-dependent inflammasome activation and transcriptional efferocytic response of macrophages.

On a daily basis, over 100 billion white and red blood cells are turned over through efferocytosis to prevent the inflammatory consequences associated with the accumulation of apoptotic debris and to maintain tissue homeostasis.[8,26] Although the splenomegaly of LIPA-deficient mice has been associated with extramedullary hematopoiesis,[12] the spleen does not support hematopoiesis in humans under injury-free conditions,[50] arguing that defective efferocytosis is most likely the culprit of the inflammatory phenotype and splenomegaly of LIPA mutation carriers.[11] Considerable data support that dying cells are normally phagocytosed by macrophages in the spleen and liver, and apoptotic bodies are rapidly broken down into their molecular constituents, including iron and lipids, which must be recycled or transported back into the circulation.[39,40] Challenging mice with stressed RBCs or ALs revealed that LIPA inhibition attenuated the efferocytic capacity of not only RPMs but also KCs. Under hypercholesterolemic disease conditions, we found that LIPA inhibition caused the spontaneous accumulation of iron in the spleen along with enhanced splenic IL-1β content. These findings could have major relevance not only for current enzyme replacement therapy for LIPA mutation carriers but also to better elucidate the recent genome-wide association studies that have reinforced LIPA as a susceptibility gene for cardiovascular diseases along with reduced LIPA activity.[51,52]

Supplementary Material

Refer to Web version on PubMed Central for supplementary material.

Acknowledgments

We thank Dr Wanida Ruangsiriluk for providing lysosomal acid lipase (LIPA)–overexpressing THP-1 macrophages and very useful scientific discussion and advice. We thank Dr Fréderic Larbret for assistance with flow cytometry and Dr Véronique Corcelle for assistance in animal facilities.

Sources of Funding

The Fondation ARC (Association pour la Recherche sur le Cancer; RAC15014AAA) and the Austrian Science Fund (W1226 DK-MCD) support L. Boyer and D. Kratky, respectively. PACA region PhD fellowship supports M. Viaud, and BioTechMed-Graz (Flagship) supports N. Vujic and M. Duta-Mare fellowships. BioTechMed-Graz (Flagship Lipases and Lipid Signaling) supports D. Kratky. This work was supported by the Inserm Atip-Avenir program, the association VML (Vaincre les Maladies Lysosomales), the European Marie Curie Career Integration Grant (CIG-630926), and the Agence Nationale de la Recherche (ANR-14-CE12-0017-01) to L. Yvan-Charvet.

Nonstandard Abbreviations and Acronyms

AL	apoptotic lymphocytes
ER	endoplasmic reticulum
GRP78	78 kDa glucose-regulated protein
HDL	high-density lipoprotein
IL	interleukin
IP3R	inositol trisphosphate receptor
KC	Kupffer cells
LAP	microtubule-associated protein 1A/1B-light chain 3 (LC3)-associated phagocytosis
LDL	low-density lipoprotein
LIPA	lysosomal acid lipase
LXR	liver X receptor
MAM	mitochondria-associated membrane
NLRP3	NOD-like receptor family, pyrin domain containing
NOX2	Nicotinamide adenine dinucleotide phosphate (NADPH) oxidase 2
OHC	hydroxycholesterol
Rac1	Ras-related C3 botulinum toxin substrate 1
ROS	reactive oxygen species
RPMs	red pulp macrophages
TFEB	transcription factor E-box
TRPML1	transient receptor potential channel 1

References

1. Wynn TA, Chawla A, Pollard JW. Macrophage biology in development, homeostasis and disease. Nature. 2013; 496:445–455. DOI: 10.1038/nature12034 [PubMed: 23619691]
2. Tall AR, Yvan-Charvet L. Cholesterol, inflammation and innate immunity. Nat Rev Immunol. 2015; 15:104–116. DOI: 10.1038/nri3793 [PubMed: 25614320]
3. Han CZ, Ravichandran KS. Metabolic connections during apoptotic cell engulfment. Cell. 2011; 147:1442–1445. DOI: 10.1016/j.cell.2011.12.006 [PubMed: 22196723]
4. Nagata S, Hanayama R, Kawane K. Autoimmunity and the clearance of dead cells. Cell. 2010; 140:619–630. DOI: 10.1016/j.cell.2010.02.014 [PubMed: 20211132]
5. Maxfield FR, Tabas I. Role of cholesterol and lipid organization in disease. Nature. 2005; 438:612–621. DOI: 10.1038/nature04399 [PubMed: 16319881]
6. Goldstein JL, DeBose-Boyd RA, Brown MS. Protein sensors for membrane sterols. Cell. 2006; 124:35–46. DOI: 10.1016/j.cell.2005.12.022 [PubMed: 16413480]
7. Spann NJ, Glass CK. Sterols and oxysterols in immune cell function. Nat Immunol. 2013; 14:893–900. DOI: 10.1038/ni.2681 [PubMed: 23959186]
8. Tabas I. Macrophage death and defective inflammation resolution in atherosclerosis. Nat Rev Immunol. 2010; 10:36–46. DOI: 10.1038/nri2675 [PubMed: 19960040]
9. Duewell P, Kono H, Rayner KJ, et al. NLRP3 inflammasomes are required for atherogenesis and activated by cholesterol crystals. Nature. 2010; 464:1357–1361. DOI: 10.1038/nature08938 [PubMed: 20428172]
10. Zelcer N, Tontonoz P. Liver X receptors as integrators of metabolic and inflammatory signaling. J Clin Invest. 2006; 116:607–614. DOI: 10.1172/JCI27883 [PubMed: 16511593]
11. Bernstein DL, Hülkova H, Bialer MG, Desnick RJ. Cholesteryl ester storage disease: review of the findings in 135 reported patients with an underdiagnosed disease. J Hepatol. 2013; 58:1230–1243. DOI: 10.1016/j.jhep.2013.02.014 [PubMed: 23485521]
12. Du H, Grabowski GA. Lysosomal acid lipase and atherosclerosis. Curr Opin Lipidol. 2004; 15:539–544. [PubMed: 15361789]
13. Yan C, Lian X, Li Y, Dai Y, White A, Qin Y, Li H, Hume DA, Du H. Macrophage-specific expression of human lysosomal acid lipase corrects inflammation and pathogenic phenotypes in lal −/− mice. Am J Pathol. 2006; 169:916–926. DOI: 10.2353/ajpath.2006.051327 [PubMed: 16936266]
14. Huang SC, Everts B, Ivanova Y, et al. Cell-intrinsic lysosomal lipolysis is essential for alternative activation of macrophages. Nat Immunol. 2014; 15:846–855. DOI: 10.1038/ni.2956 [PubMed: 25086775]
15. Ouimet M, Franklin V, Mak E, Liao X, Tabas I, Marcel YL. Autophagy regulates cholesterol efflux from macrophage foam cells via lysosomal acid lipase. Cell Metab. 2011; 13:655–667. DOI: 10.1016/j.cmet.2011.03.023 [PubMed: 21641547]
16. Razani B, Feng C, Coleman T, Emanuel R, Wen H, Hwang S, Ting JP, Virgin HW, Kastan MB, Semenkovich CF. Autophagy links inflammasomes to atherosclerotic progression. Cell Metab. 2012; 15:534–544. DOI: 10.1016/j.cmet.2012.02.011 [PubMed: 22440612]
17. Sheedy FJ, Grebe A, Rayner KJ, Kalantari P, Ramkhelawon B, Carpenter SB, Becker CE, Ediriweera HN, Mullick AE, Golenbock DT, Stuart LM, Latz E, Fitzgerald KA, Moore KJ. CD36 coordinates NLRP3 inflammasome activation by facilitating intracellular nucleation of soluble ligands into particulate ligands in sterile inflammation. Nat Immunol. 2013; 14:812–820. DOI: 10.1038/ni.2639 [PubMed: 23812099]
18. Green DR, Oguin TH, Martinez J. The clearance of dying cells: table for two. Cell Death Differ. 2016; 23:915–926. DOI: 10.1038/cdd.2015.172 [PubMed: 26990661]
19. Yvan-Charvet L, Pagler TA, Seimon TA, Thorp E, Welch CL, Witztum JL, Tabas I, Tall AR. ABCA1 and ABCG1 protect against oxidative stress-induced macrophage apoptosis during efferocytosis. Circ Res. 2010; 106:1861–1869. DOI: 10.1161/CIRCRESAHA.110.217281 [PubMed: 20431058]
20. Emanuel R, Sergin I, Bhattacharya S, Turner J, Epelman S, Settembre C, Diwan A, Ballabio A, Razani B. Induction of lysosomal biogenesis in atherosclerotic macrophages can rescue lipid-

induced lysosomal dysfunction and downstream sequelae. Arterioscler Thromb Vasc Biol. 2014; 34:1942–1952. DOI: 10.1161/ATVBAHA.114.303342 [PubMed: 25060788]

21. Sergin I, Evans TD, Zhang X, et al. Exploiting macrophage autophagy-lysosomal biogenesis as a therapy for atherosclerosis. Nat Commun. 2017; 8:15750.doi: 10.1038/ncomms15750 [PubMed: 28589926]
22. Settembre C, Di Malta C, Polito VA, Garcia Arencibia M, Vetrini F, Erdin S, Erdin SU, Huynh T, Medina D, Colella P, Sardiello M, Rubinsztein DC, Ballabio A. TFEB links autophagy to lysosomal biogenesis. Science. 2011; 332:1429–1433. DOI: 10.1126/science.1204592 [PubMed: 21617040]
23. Weissmann G. The role of lysosomes in inflammation and disease. Annu Rev Med. 1967; 18:97–112. DOI: 10.1146/annurev.me.18.020167.000525 [PubMed: 5337539]
24. Lamkanfi M, Dixit VM. In retrospect: the inflammasome turns 15. Nature. 2017; 548:534–535. DOI: 10.1038/548534a [PubMed: 28858314]
25. Sokolovska A, Becker CE, Ip WK, Rathinam VA, Brudner M, Paquette N, Tanne A, Vanaja SK, Moore KJ, Fitzgerald KA, Lacy-Hulbert A, Stuart LM. Activation of caspase-1 by the NLRP3 inflammasome regulates the NADPH oxidase NOX2 to control phagosome function. Nat Immunol. 2013; 14:543–553. DOI: 10.1038/ni.2595 [PubMed: 23644505]
26. Elliott MR, Ravichandran KS. The dynamics of apoptotic cell clearance. Dev Cell. 2016; 38:147–160. DOI: 10.1016/j.devcel.2016.06.029 [PubMed: 27459067]
27. Giaever I, Keese CR. A morphological biosensor for mammalian cells. Nature. 1993; 366:591–592. DOI: 10.1038/366591a0 [PubMed: 8255299]
28. Zhou R, Yazdi AS, Menu P, Tschopp J. A role for mitochondria in NLRP3 inflammasome activation. Nature. 2011; 469:221–225. DOI: 10.1038/nature09663 [PubMed: 21124315]
29. Brookes PS, Yoon Y, Robotham JL, Anders MW, Sheu SS. Calcium, ATP, and ROS: a mitochondrial love-hate triangle. Am J Physiol Cell Physiol. 2004; 287:C817–C833. DOI: 10.1152/ajpcell.00139.2004 [PubMed: 15355853]
30. Horng T. Calcium signaling and mitochondrial destabilization in the triggering of the NLRP3 inflammasome. Trends Immunol. 2014; 35:253–261. DOI: 10.1016/j.it.2014.02.007 [PubMed: 24646829]
31. Lloyd-Evans E, Morgan AJ, He X, Smith DA, Elliot-Smith E, Sillence DJ, Churchill GC, Schuchman EH, Galione A, Platt FM. Niemann-Pick disease type C1 is a sphingosine storage disease that causes deregulation of lysosomal calcium. Nat Med. 2008; 14:1247–1255. DOI: 10.1038/nm.1876 [PubMed: 18953351]
32. Sano R, Annunziata I, Patterson A, Moshiach S, Gomero E, Opferman J, Forte M, d'Azzo A. GM1-ganglioside accumulation at the mitochondria-associated ER membranes links ER stress to Ca(2+)-dependent mitochondrial apoptosis. Mol Cell. 2009; 36:500–511. DOI: 10.1016/j.molcel.2009.10.021 [PubMed: 19917257]
33. Shen D, Wang X, Li X, Zhang X, Yao Z, Dibble S, Dong XP, Yu T, Lieberman AP, Showalter HD, Xu H. Lipid storage disorders block lysosomal trafficking by inhibiting a TRP channel and lysosomal calcium release. Nat Commun. 2012; 3:731.doi: 10.1038/ncomms1735 [PubMed: 22415822]
34. Prasad M, Pawlak KJ, Burak WE, Perry EE, Marshall B, Whittal RM, Bose HS. Mitochondrial metabolic regulation by GRP78. Sci Adv. 2017; 3:e1602038.doi: 10.1126/sciadv.1602038 [PubMed: 28275724]
35. Reboldi A, Dang EV, McDonald JG, Liang G, Russell DW, Cyster JG. Inflammation. 25-Hydroxycholesterol suppresses interleukin-1-driven inflammation downstream of type I interferon. Science. 2014; 345:679–684. DOI: 10.1126/science.1254790 [PubMed: 25104388]
36. Dang EV, McDonald JG, Russell DW, Cyster JG. Oxysterol restraint of cholesterol synthesis prevents AIM2 inflammasome activation. Cell. 2017; 171:1057.e11–1071.e11. DOI: 10.1016/j.cell.2017.09.029 [PubMed: 29033131]
37. Gonzalez A-N, Bensinger SJ, Hong C, Beceiro S, Bradley MN, Zelcer N, Deniz J, Ramirez C, Díaz M, Gallardo G, et al. Apoptotic cells promote their own clearance and immune tolerance through activation of the nuclear receptor LXR. Immunity. 2009; 31:245–258. [PubMed: 19646905]

38. Theurl I, Hilgendorf I, Nairz M, et al. On-demand erythrocyte disposal and iron recycling requires transient macrophages in the liver. Nat Med. 2016; 22:945–951. DOI: 10.1038/nm.4146 [PubMed: 27428900]
39. De Domenico I, McVey Ward D, Kaplan J. Regulation of iron acquisition and storage: consequences for iron-linked disorders. Nat Rev Mol Cell Biol. 2008; 9:72–81. DOI: 10.1038/nrm2295 [PubMed: 17987043]
40. Kohyama M, Ise W, Edelson BT, Wilker PR, Hildner K, Mejia C, Frazier WA, Murphy TL, Murphy KM. Role for Spi-C in the development of red pulp macrophages and splenic iron homeostasis. Nature. 2009; 457:318–321. DOI: 10.1038/nature07472 [PubMed: 19037245]
41. Jais A, Einwallner E, Sharif O, et al. Heme oxygenase-1 drives metaflammation and insulin resistance in mouse and man. Cell. 2014; 158:25–40. DOI: 10.1016/j.cell.2014.04.043 [PubMed: 24995976]
42. Sarrazy V, Sore S, Viaud M, Rignol G, Westerterp M, Ceppo F, Tanti JF, Guinamard R, Gautier EL, Yvan-Charvet L. Maintenance of macrophage redox status by ChREBP limits inflammation and apoptosis and protects against advanced atherosclerotic lesion formation. Cell Rep. 2015; 13:132–144. DOI: 10.1016/j.celrep.2015.08.068 [PubMed: 26411684]
43. Kellner-Weibel G, Yancey PG, Jerome WG, Walser T, Mason RP, Phillips MC, Rothblat GH. Crystallization of free cholesterol in model macrophage foam cells. Arterioscler Thromb Vasc Biol. 1999; 19:1891–1898. [PubMed: 10446067]
44. Scialò F, Fernández-Ayala DJ, Sanz A. Role of mitochondrial reverse electron transport in ROS signaling: potential roles in health and disease. Front Physiol. 2017; 8:428.doi: 10.3389/fphys.2017.00428 [PubMed: 28701960]
45. Wang Y, Subramanian M, Yurdagul A Jr, Barbosa-Lorenzi VC, Cai B, de Juan-Sanz J, Ryan TA, Nomura M, Maxfield FR, Tabas I. Mitochondrial fission promotes the continued clearance of apoptotic cells by macrophages. Cell. 2017; 171:331.e22–345.e22. DOI: 10.1016/j.cell.2017.08.041 [PubMed: 28942921]
46. Kanerva K, Uronen RL, Blom T, Li S, Bittman R, Lappalainen P, Peränen J, Raposo G, Ikonen E. LDL cholesterol recycles to the plasma membrane via a Rab8a-Myosin5b-actin-dependent membrane transport route. Dev Cell. 2013; 27:249–262. DOI: 10.1016/j.devcel.2013.09.016 [PubMed: 24209575]
47. Fond AM, Lee CS, Schulman IG, Kiss RS, Ravichandran KS. Apoptotic cells trigger a membrane-initiated pathway to increase ABCA1. J Clin Invest. 2015; 125:2748–2758. DOI: 10.1172/JCI80300 [PubMed: 26075824]
48. Frolov A, Zielinski SE, Crowley JR, Dudley-Rucker N, Schaffer JE, Ory DS. NPC1 and NPC2 regulate cellular cholesterol homeostasis through generation of low density lipoprotein cholesterol-derived oxysterols. J Biol Chem. 2003; 278:25517–25525. DOI: 10.1074/jbc.M302588200 [PubMed: 12719428]
49. Zhang JR, Coleman T, Langmade SJ, Scherrer DE, Lane L, Lanier MH, Feng C, Sands MS, Schaffer JE, Semenkovich CF, Ory DS. Niemann-Pick C1 protects against atherosclerosis in mice via regulation of macrophage intracellular cholesterol trafficking. J Clin Invest. 2008; 118:2281–2290. DOI: 10.1172/JCI32561 [PubMed: 18483620]
50. Crosby WH. Hematopoiesis in the human spleen. Arch Intern Med. 1983; 143:1321–1322. [PubMed: 6870401]
51. Wild PS, Zeller T, Schillert A, et al. A genome-wide association study identifies LIPA as a susceptibility gene for coronary artery disease. Circ Cardiovasc Genet. 2011; 4:403–412. DOI: 10.1161/CIRCGENETICS.110.958728 [PubMed: 21606135]
52. Morris GE, Braund PS, Moore JS, Samani NJ, Codd V, Webb TR. Coronary artery disease-associated LIPA coding variant rs1051338 reduces lysosomal acid lipase levels and activity in lysosomes. Arterioscler Thromb Vasc Biol. 2017; 37:1050–1057. DOI: 10.1161/ATVBAHA.116.308734 [PubMed: 28279971]

Novelty and Significance

What Is Known?

- Macrophages accumulate a substantial amount of cholesterol after the ingestion of apoptotic cells.
- LIPA (lysosomal acid lipase) is an endocytic enzyme that hydrolyzes cholesteryl esters into free cholesterol.
- LIPA deficiency causes macrophage foam cell formation and tissue inflammatory phenotypes.

What New Information Does This Article Contribute?

- LIP A hydrolyzes cholesteryl esters from ingested apoptotic allowing efficient oxysterol production to transcriptionally prime macrophages for cholesterol efflux and clearance of apoptotic cells via liver X receptor activation.
- LIPA allows 25-hydroxycholesterol generation to repurpose mitochondrial metabolism, preventing activation of the Nlrp3 (NOD-like receptor family, pyrin domain containing) inflammasome and Rac1 (Ras-related C3 botulinum toxin substrate 1)-dependent phagocytic cup disassembly.
- LIPA orchestrates disposal of stressed erythrocytes and apoptotic lymphocytes in vivo.

Everyday, billions of dying cells are phagocytosed through efferocytosis to prevent the inflammatory consequences associated with the accumulation of apoptotic debris. Therefore, it has been proposed that defective efferocytosis impairs tissue homeostasis. Here, we found that LIPA-dependent lysosomal cholesterol hydrolysis is essential to maintain an efficient efferocytic response. In vivo, defective clearance of stressed erythrocytes and apoptotic lymphocytes after LIPA inhibition led to an enhanced inflammatory response, culminating in splenomegaly under hypercholesterolemia. Thus, by controlling lysosomal cholesterol hydrolysis, LiPA links the macrophage efferocytic response to chronic inflammation.

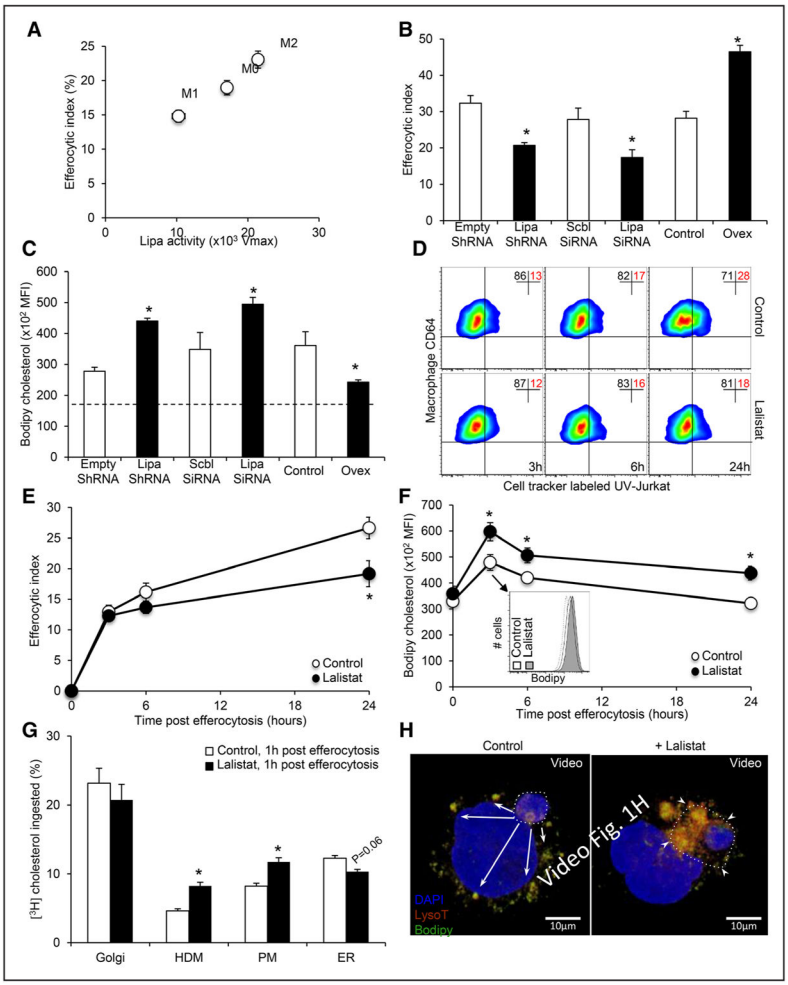

Figure 1. LIPA (lysosomal acid lipase) expression controls efferocytic capacity and lysosomal cholesterol trafficking

A, Correlations between LIPA activity and the efferocytic index in human THP-1 macrophages exposed for 16 hours to medium alone (M0), 50 ng/mL lipopolysaccharide (LPS; M1) or 15 ng/mL IL (interleukin)-4 (M2). **B**, THP-1 macrophages were transduced with empty or LIPA ShRNA lentiviral particles or transfected with scrambled (Scbl) or LIPA SiRNA before incubation with CellTracker Deep Red-prelabeled apoptotic Jurkat cells (ultra-violet or UV-Jurkat) and quantification of the efferocytic index by flow cytometry. LIPA-overexpressing cells (Ovex) were also used in this assay. **C**, BODIPY (bore-dipyrromethene) staining was quantified by flow cytometry in THP-1 macrophages after modulation of LIPA expression (as described above) and exposure for 30 minutes to apoptotic Jurkat cells. Data are expressed as the mean fluorescence intensity (MFI). The dotted line represents the BODIPY-neutral lipid content into nonefferocytic control cells. **D**, **E**, THP-1 macrophages ($CD64^{+}$) were incubated for the indicated times in the presence or absence of 10 µmol/L lalistat together with CellTracker Deep Red-prelabeled apoptotic Jurkat cells, and the efferocytic index was quantified by flow cytometry. **F**, THP-1 macrophages incubated in the presence or absence of 10 µmol/L lalistat were stimulated with apoptotic Jurkat cells for the indicated times. BODIPY staining was quantified by flow

cytometry. Inset depicts a representative histogram at the indicated time point. **G**, Control or lalistat-treated THP-1 efferocytes, cultured for 1 hour after the ingestion of [^{3}H]-cholesterol–prelabeled apoptotic Jurkat cells, were fractionated by sucrose step gradient, and fractions were assayed for [^{3}H]-cholesterol incorporation as described in the Methods section. **H**, Representative 3-dimensional reconstruction from confocal Z-stack images of an ingested apoptotic cell prelabeled with BODIPY (green) and localized within a phagolysosome (stained with LysoTracker Deep Red). Cells were counterstained with DAPI (nuclear staining). Arrows indicate BODIPY clusters in phagocytic cells (8–10 different confocal images were analyzed per condition from experiments performed in triplicate). The data are given as the mean±SEM of at least 2 experiments performed in triplicate. *P<0.05 vs controls. ER indicates endoplasmic reticulum.

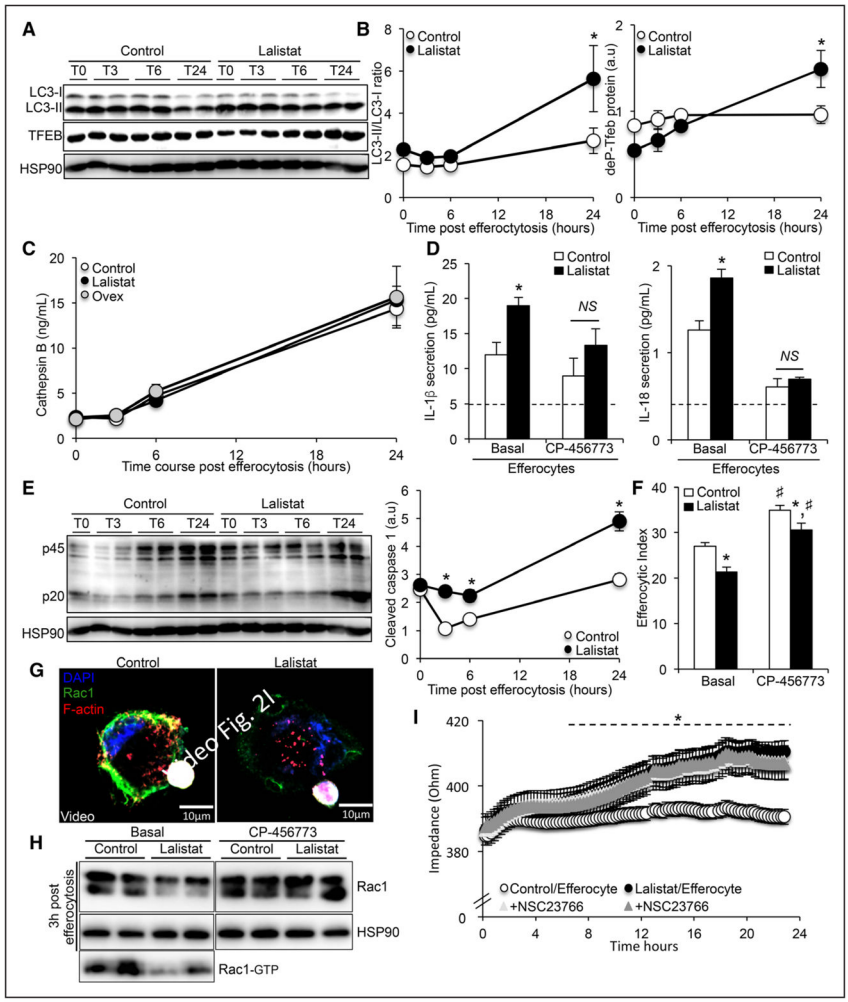

Figure 2. Defective lysosomal cholesterol hydrolysis promotes lysosomal damage–independent inflammasome activation after efferocytosis causing subsequent Rac1 (Ras-related C3 botulinum toxin substrate 1)-dependent phagocytic cup defects

A, Representative immunoblots of LC3I/II and phospho-Tfeb (transcription factor E-box) from control or lalistat-treated THP-1 macrophages incubated for 30 minutes with apoptotic Jurkat cells and cultured for various times. **B**, Kinetics of band densities normalized to HSP90 (heat shock protein 90) are shown for the indicated times. **C**, Cathepsin B secretion levels from control or lalistat-treated THP-1 efferocytes cultured for the indicated times after the ingestion of apoptotic cells and expressed in ng/mL. **D**, IL (interleukin)-1β and IL-18 secretion levels (expressed in pg/mL) from control or lalistat-treated THP-1 efferocytes cultured for 3 hours after the ingestion of apoptotic cells in the presence or absence of 25 nmol/L Nlrp3 (NOD-like receptor family, pyrin domain containing) inflammasome inhibitor (CP456773). The dotted lines represent IL-1β and IL-18 secretion levels into nonefferocytic control cells. **E**, Immunoblot of caspase-1 from control or lalistat-treated THP-1 macrophages incubated for 30 minutes with apoptotic Jurkat cells and cultured for various times and quantification of cleaved caspase-1. **F**, Control and lalistat-treated THP-1 macrophages were incubated in the presence or absence of 25 nmol/L Nlrp3 inflammasome inhibitor (CP456773) together with CellTracker Red-prelabeled apoptotic Jurkat cells, and

the efferocytic index was quantified by flow cytometry 16 hours later. **G**, THP-1 macrophages incubated in the presence or absence of 10 μmol/L lalistat were stimulated with CellTracker Deep Red-prelabeled apoptotic Jurkat cells for 30 minutes. After an additional culture period, the cells were counterstained with Rac1 (green), F-actin (red), and DAPI (nuclear staining); a 3-dimensional reconstruction from confocal Z-stack images is provided. **H**, Immunoblots of Rac1 from control or lalistat-treated THP-1 macrophages cultured for 3 hours after the ingestion of apoptotic Jurkat cells in presence or absence of 25 nmol/L of the Nlrp3 inflammasome inhibitor (CP-456773). Rac1-GTP is for Rac1 bind to GTP, the active form of Rac1. **I**, Real-time evaluation of macrophage protrusion dynamics by impedance reading of control or lalistat-treated THP-1 efferocytes in presence or absence of the Rac1 inhibitor, NSC23766. The data are given as the mean±SEM of 2 to 5 independent experiments performed in triplicate. *P<0.05 vs controls. #P<0.05 treatment effect. a.u. indicates arbitrary units.

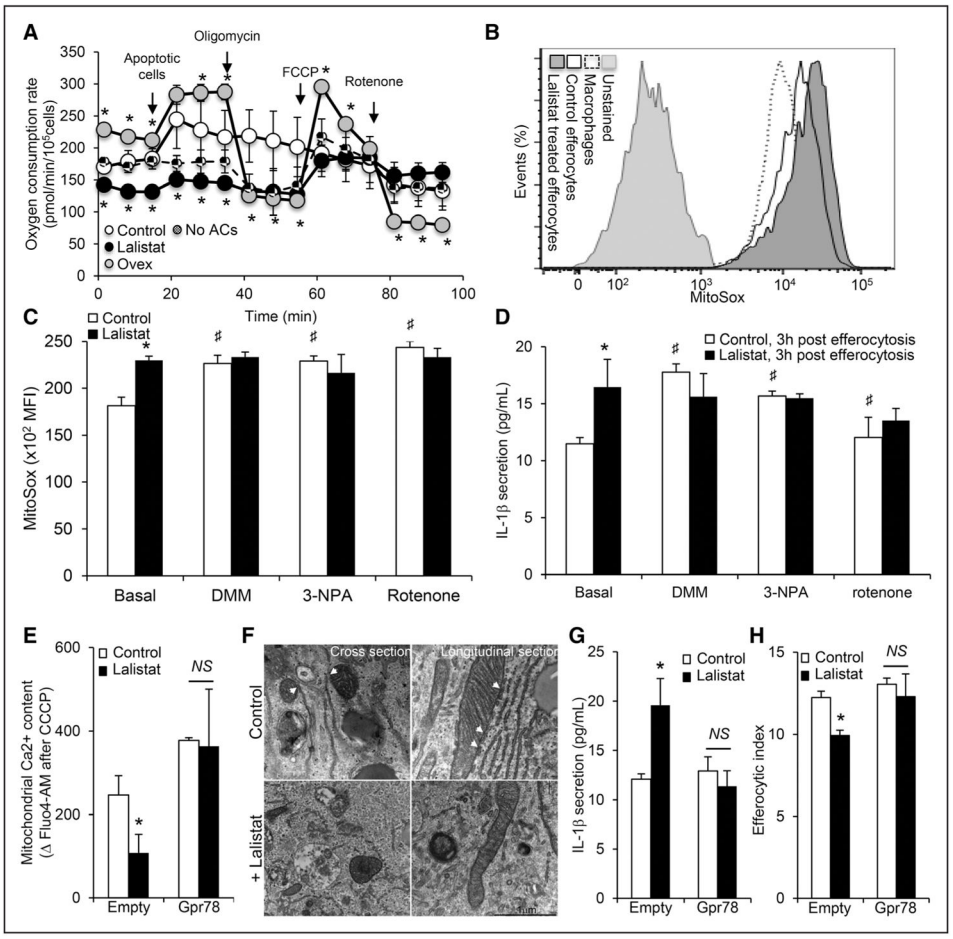

Figure 3. Defective lysosomal cholesterol hydrolysis restrains mitochondria-associated membrane (MAM)–dependent mitochondrial metabolic repurposing after efferocytosis to activate the inflammasome and subsequent efferocytic defects

A, Oxygen consumption rate (OCR) recordings of control, lalistat-treated, or LIPA (lysosomal acid lipase)-overexpressing (Ovex) THP-1 macrophages under the indicated conditions. **B**, Representative histograms and (**C**) quantification of mitochondrial reactive oxygen species (ROS) generation using the MitoSox probe by flow cytometry in control and lalistat-treated THP-1 efferocytes cultured for 3 hours after ingestion of apoptotic cells in the presence or absence of 10 mmol/L of the succinate oxidation inhibitor (dimethyl malonate [DMM]) or 1 μmol/L of the succinate dehydrogenase inhibitor (3-nitropropionic acid [3-NPA]) or 1 μmol/L of rotenone. Data are expressed as mean fluorescence intensity (MFI). **D**, IL (interleukin)-1β secretion levels in these cells at the end of the incubation period. **E**, THP-1 macrophages were transduced with empty or GPR78 overexpressing adenoviral particles and loaded for 30 minutes with the fluorescent calcium probe Fluo4-AM (acetoxymethyl) before the start of the efferocytosis experiment. Control and lalistat-treated THP-1 macrophages were then incubated for 30 minutes with apoptotic Jurkat cells before treatment with carbonyl cyanide 3-chlorophenylhydrazone (CCCP) to release mitochondrial calcium. Mitochondrial calcium content was calculated as the difference in mean fluorescence intensity between conditions treated with or without CCCP. **F**, Representative transmission electron microscopy images of control or lalistat-treated THP-1 efferocytes

showing endoplasmic reticulum (ER)–mitochondria contacts (scale bar, 1 μm). **G**, IL-1β secretion levels (**H**) and efferocytic index from control and GPR78 overexpressing THP-1 macrophages incubated in the presence or absence of 10 μmol/L lalistat and cultured for 3 hours after the ingestion of apoptotic Jurkat cells. The results are expressed as the mean ±SEM of at least 2 independent experiments performed in triplicate. **P*<0.05 vs controls. #*P*<0.05 treatment effect. AC indicates apoptotic cell.

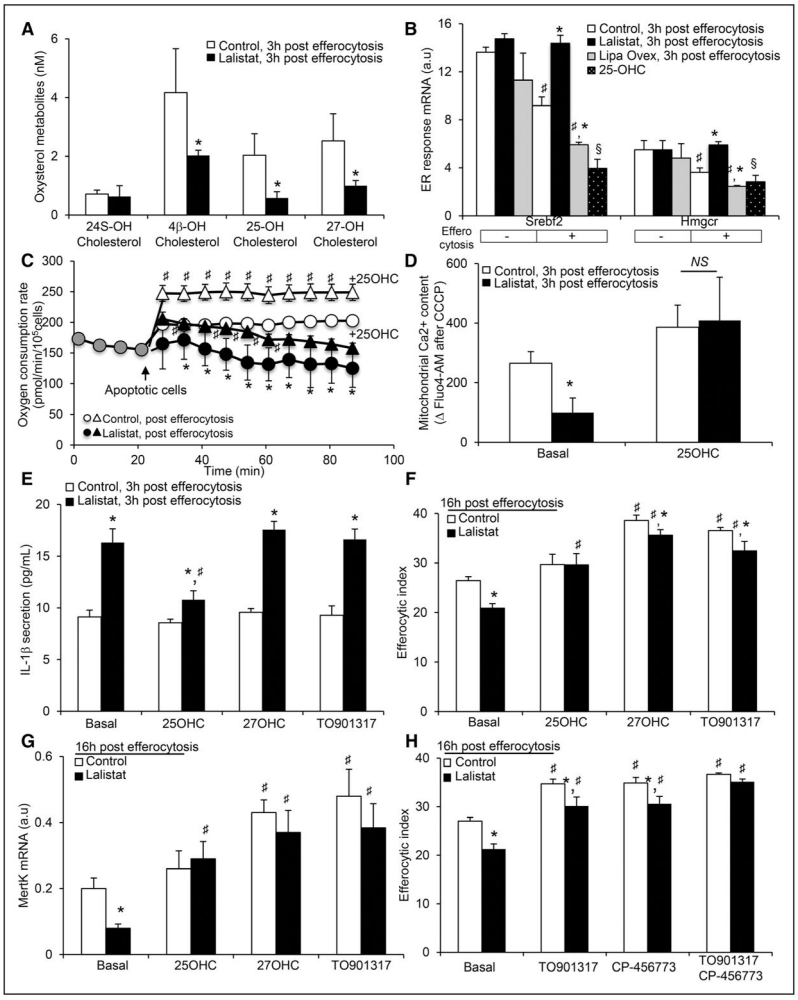

Figure 4. Lysosomal cholesterol hydrolysis governs the efferocytic response by controlling oxysterol production

A, Oxysterol metabolites (24S-, 4β-, 25- and 27-hydroxy(OH)cholesterol) were determined by liquid chromatography-mass spectrometry (LC-MS). **B**, Effects of LIPA (lysosomal acid lipase) inhibition, LIPA overexpression, and 25-OHC treatment (5 μmol/L) on *Srebf2* and *Hmgcr* mRNA expression in THP-1 macrophages 3 hours post-efferocytosis. Quantified transcript levels (normalized to m36B4) are expressed in arbitrary units (a.u.). **C**, Oxygen consumption rate (OCR) recordings of control and lalistat-treated THP-1 efferocytes in the presence or absence of 5 μmol/L 25-OHC. **D**, Control and lalistat-treated THP-1 macrophages, preloaded for 30 minutes with the fluorescent calcium probe Fluo4-AM (acetoxymethyl), were incubated for 30 minutes with apoptotic Jurkat cells in presence or absence of 5 μmol/L 25-OHC. Release of mitochondrial calcium was achieved at the end of the experiment by treating cells with carbonyl cyanide 3-chlorophenylhydrazone (CCCP). Mitochondrial calcium content was calculated as the difference in mean fluorescence intensity between conditions treated with or without CCCP. **E**, IL-1β secretion levels from control or lalistat-treated THP-1 efferocytes cultured for 3 hours after the ingestion of apoptotic cells in the presence or absence of 5 μmol/L 25-OHC, 5 μmol/L 27-OHC or 3 μmol/L LXR agonist (TO901317). **F**, Control and lalistat-treated THP-1 macrophages were

incubated under the same conditions as described above, and the efferocytic index was quantified by flow cytometry 16 hours later. **G**, MertK transcript levels (normalized to m36B4) were determined under the same conditions as described in **F** and expressed in a.u. **H**, Control and lalistat-treated THP-1 macrophages were incubated in the presence or absence of 3 μmol/L liver X receptor (LXR) agonist (TO901317) and 25 nmol/L Nlrp3 (NOD-like receptor family, pyrin domain containing) inflammasome inhibitor (CP-456773) together with CellTracker Red-prelabeled apoptotic Jurkat cells and the efferocytic index was quantified by flow cytometry 16 hours later. The results are expressed as the mean ±SEM of 2 to 5 independent experiments. **P*<0.05 vs controls. #*P*<0.05 treatment effect.

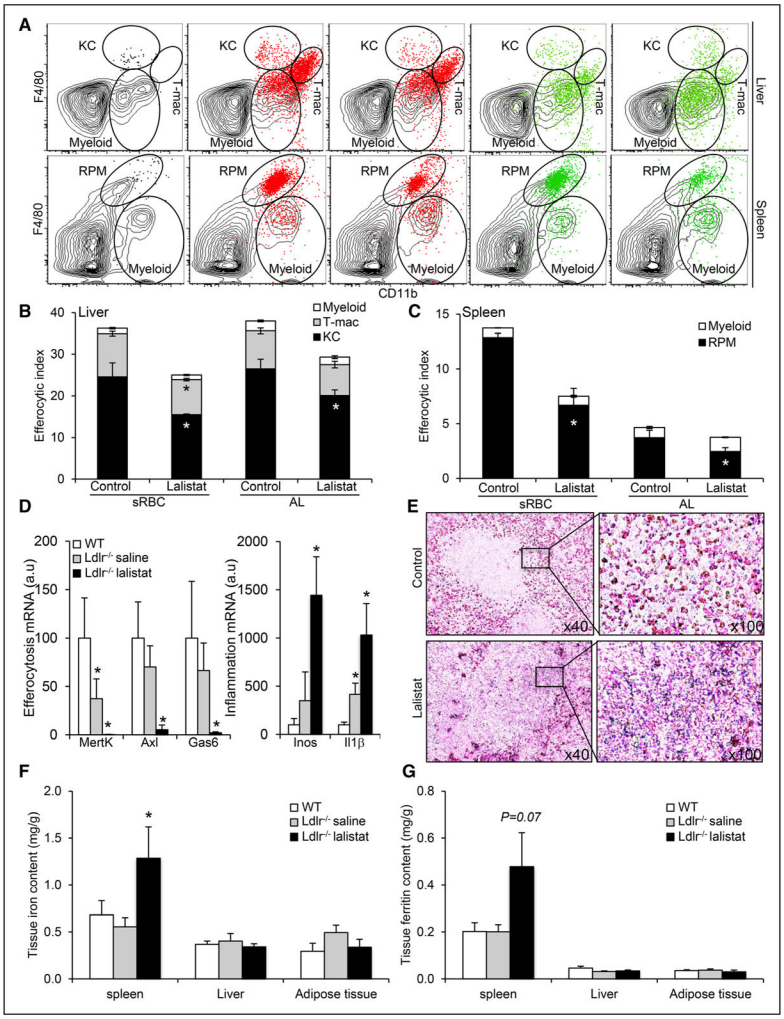

Figure 5. Inhibition of lysosomal lipid hydrolysis promotes defective efferocytosis in vivo leading to pathogenic inflammation and splenic iron deposition under hypercholesterolemia

A, Representative dot plots of gating for F4/80^{high}CD11b^{int} KCs, F4/80^{low}CD11b^{high} myeloid cells, and F4/80^{high}CD11b^{high} tMΦ in the liver (**top**) and F4/80^{high}CD11b^{int} RPMs and F4/80^{low}CD11b^{high} myeloid cells in the spleen (**bottom**) 16 hours after intravenous injection of CellTracker^{+} stressed erythrocytes (stressed red blood cells [sRBCs], red) or apoptotic lymphocytes (ALs; UV-T, green). Black dot plots represent cells gated on CD45^{+} leukocytes in the liver and spleen, and the red or green dot plot overlays show CellTracker^{+} cells. Quantification of (**B**, **C**) the efferocytic index of each cell type in the liver (myeloid, transient macrophage population [T-mac], and ketocholesterol [KC]) or the spleen (myeloid and RPM). **D**, mRNA expression of efferocytic and inflammatory markers in 12-week high-fat-fed wild-type (WT) or *Ldlr*$^{-/-}$ mice treated for the past 2 weeks with subcutaneous injections of either saline or 20 mg/kg lalistat every 2 days. **E**, Perl's Prussian stain for ferric iron in the spleens of these mice (original magnification, 40× and 100×). **F**, Iron levels and (**G**) ferritin levels in spleen, liver, and adipose tissue of WT or saline and lalistat-treated *Ldlr*$^{-/-}$ mice on a high-fat diet. The data are expressed as the mean±SEM of 4 to 6 animals per group. *P<0.05 vs saline-injected control or *Ldlr*$^{-/-}$ mice.

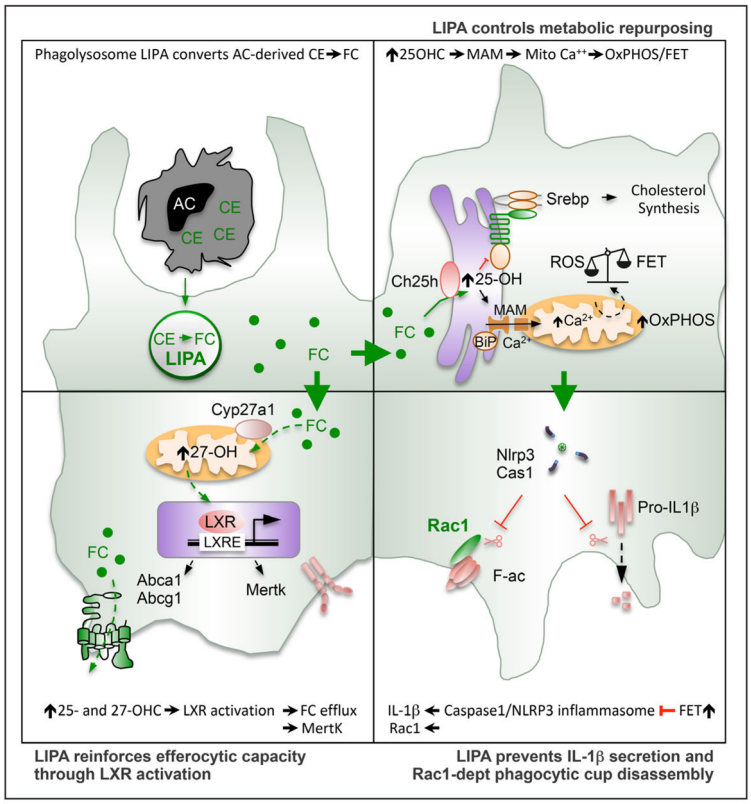

Figure 6.
Graphical abstract.

Table

Effects of Lalistat Treatment on Metabolic and Inflammatory Markers

	Saline-Treated Ldr$^{-/-}$	Lalistat-Treated Ldr$^{-/-}$
Body weight, g	24.97±0.32	24.60±1.02
Epididymal adipose tissue, mg	563±133	485±98
Spleen, mg	109±13	178±37*
Plasma cholesterol levels, mg/mL	2.14±0.26	2.18±0.25
Plasma triglyceride levels, mg/mL	3.69±0.85	4.42±0.19
Plasma ALT levels, U/L	8.71±1.24	9.77±0.64
Plasma AST levels, U/L	16.31±3.48	17.63±0.31
Plasma BUN levels, mg/dL	13.7±3.2	16.5±1.5
Plasma cystatin C levels, mg/L	0.11±0.01	0.11±0.01
Plasma iron levels, mg/L	6.19±1.77	6.49±1.44
Plasma ferritin levels, mg/L	0.34±0.03	0.34±0.01
Plasma IL-1b levels, pg/mL	ND	21.5±5.9
Splenic IL-1b content, pg/mg protein	114±29	331±37*

ALT indicates alanine aminotransferase; AST, aspartate aminotransferase; BUN, blood urea nitrogen; IL, interleukin; and ND, not determined.

*P<0.05 vs saline-treated mice.